

Optimal Guidance Trajectories for a Nanosat Docking with a Non-Cooperative Resident Space Object

Parv Patel
University of Southern California
Los Angeles, CA 90089
404-452-9090
parvpate@usc.edu

Bogdan Udrea
VisSidus Technologies Inc.
Daytona Beach, FL 32114
206-227-8075
bogdan.udrea@vissidus.com

Abstract—There has been an increasing interest in on-orbit autonomous servicing and repair of satellites as well as controlled active debris removal (ADR) in the space industry recently. One of the most challenging tasks for servicing/repair as well as for ADR is the rendezvous and docking with a non-cooperative tumbling resident space object (RSO). This paper presents a propellant optimal maneuver profile for a servicing spacecraft to perform proximity operations and eventually dock with a non-cooperative target. The strategy is to find an optimal trajectory which will guide the servicing spacecraft to approach the tumbling satellite such that the two vehicles will eventually have no relative motion. Therefore, a subsequent docking or capture operation can be safely performed. The research described here elaborates on the previous work that studied the minimum-control-effort for a 3-D rendezvous to a tumbling object considering a full six-degree-of-freedom model of both chaser and target. The current work expands the scope by adding a new set of linearized equations of motion that capture not only the effect of the J_2 geopotential disturbance force but also quadratic drag force.

Typically, Hill's linearized equations of relative motion have been used for this analysis, but they fail to capture the effect of J_2 disturbance force and drag on the chaser satellite. It appears that there is a need for a set of linearized equations that are as easy and useful as Hills equations, but at the same time capture the effect of the J_2 disturbance and drag force acting on the spacecrafcts. The current paper presents a set of linearized, constant coefficient differential equations that capture the J_2 and quadratic drag perturbation. The importance of these perturbations is studied by doing trajectory propagation. Finally, it is shown for a control problem, the effect on the control-solution due to the formulated high fidelity dynamical constraints with respect to the simplified Hill's equations.

TABLE OF CONTENTS

1	INTRODUCTION	1
2	RELATIVE MOTION MODELS	2
3	EFFECTS OF PERTURBATIONS	6
4	OPTIMIZATION PROBLEM FORMULATION.....	11
5	SIMULATION RESULTS	12
6	CONCLUSION	15
	ACKNOWLEDGMENTS	15
	REFERENCES	15
	BIOGRAPHY	16

1. INTRODUCTION

There has been an increasing interest in satellite on-orbit autonomous servicing in the space industry recently. JAXA

recently completed a technology demonstration mission ETS-7 [18]. NASA did an autonomous rendezvous mission through the Demonstration for Autonomous Rendezvous Technology (DART) in 2005 [12], where the mission was not completed due to more than expected propellant usage during rendezvous maneuvering. Air Force Research Laboratory's (AFRL) Experimental Satellite Systems-10 and 11 (XSS-10 and XSS-11) have been developed in order to show the ability for a small sat to autonomously plan and rendezvous with a passive and cooperative Resident Space Object (RSO) in Low Earth Orbit (LEO) [1]. In addition, Defense Advance Research Projects Agency's (DARPA) Orbital Express (OE) Advance Technology Demonstration Program validated the technology and techniques for on-orbit refueling and configuration of two satellites [3][4]. The existence of these programs demonstrates that there is a need for a robust and effective autonomous close proximity control algorithms for multiple spacecrafcts. The use of micro-satellites to inspect, service, repair, deorbit and refuel larger spacecrafcts is a long-term goal.

In order to perform on-orbit service, the servicing spacecraft has to first rendezvous and dock with the satellite to be serviced in orbit. The tumbling of an uncontrolled resident space object (RSO) or the rotational and transnational motion of an non-cooperating RSO present challenges to the docking operations.

From a theoretical standpoint, the current research elaborates on the previous work by Boyarko et al. [5][6][7], who studied the minimum-time and minimum-control problem for a rendezvous of a chaser satellite to a tumbling object considered a full six-degree-of-freedom model of both chaser and target. The current work expands the scope by adding the effect of J_2 geopotential disturbance and the quadratic drag perturbation to investigate its effects on the proximity operations.

The majority of previous research pertaining to operations that focused on rendezvous with an uncontrolled RSO, the relative motion dynamics pertinent to proximity space operation only considers Hill's equations, also known as Clohessy-Wiltshire equations. The reason being Hills equations are very simple to implement and have been successfully used to describe the relative motion of two satellites during rendezvous maneuvers. Additionally, these linear equations have a close form solution that relates the position of the spacecrafcts with respect to their initial conditions. Because of this, they can be solved analytically and provide a solution that is fairly simple and easy to understand. These solutions also allow for an intuitive sense of the relative motion of satellites in clusters. Hill's relative equations are therefore used in the design of control laws since the most effective control schemes require a set of constant coefficient linearized differential equations. These reasons and many

978-1-4799-5380-6/15/\$31.00 ©2020 IEEE.

¹ IEEEAC Paper #2199, Version 0.1, Updated 20/10/2014.

more make them the logical first choice in describing relative spacecraft motion.

The assumption made by Hill's equations that is cited repeatedly as the main source of error is that the Earth is perfectly spherical. Because the Earth is an oblate spheroid and not a perfect sphere, the dominant effect of the asymmetry in the gravitational field is captured by the J_2 term. Not accounting for this term introduces modeling errors by the non-central forces. In the derivation of Hill's equations as seen in the later chapter, the Earth is considered spherical, and the J_2 disturbance is not incorporated. To reduce the effect of the modeling errors that are present in Hill's equations, much research has been done with varying success to incorporate the effects of the J_2 potential. Other papers do not use them at all, citing the fact that they do not capture the motion of the spacecraft correctly.

While Hill's equations have proved very useful, they have several significant limitations. Since they are linear, some error is introduced into the solution. However, linearization errors are not the only limiting factor. Hill's equations are derived under the assumption that the disturbance forces acting on the satellites are also negligible. For rendezvous missions in the low earth orbit, significant errors can be caused in the relative position due to drag. Moreover, while studying the motion of nanosatellites, which are becoming increasingly popular, there is a very strong requirement for studying the effect of drag on the spacecraft motion due to its size as even a small disturbance could cause it to drift away from its predetermined motion path. Moreover, for application concerned with proximity operations and rendezvous with non-cooperating debris, it also becomes more crucial to implement drag disturbances as a part of the relative motion as a sense of reliability, to account for all perturbations so as to not create more debris. Much work has been done to implement drag perturbations for equations of motion which are linear in velocity for single body. To model a more realistic case, this paper expands the work by implementing drag disturbance which is quadratic in velocity for the relative motion.

Detailed derivation of the linear model only encompassing the J_2 is already studied before by Patel and Udrea [13]. The model implemented the formulation of Schweighart and Sedwick [16][17] which describes the linear combination of Hill's equations with the J_2 effect. The equations derived by Schweighart and Sedwick [16][17] provide insight into the relative motion of satellites under the influence of the J_2 potential. This paper expands on the previous work by studying the effect of quadratic drag on the relative motion trajectories. Humi and Carter [8][9][10][11] presents a formulation to implement drag effects in relative motion that is linear in velocity. It also expands on the scope by implementing linear drag for non-circular or low-eccentricity elliptic reference orbits. It later presents effects of quadratic drag on orbits that are not highly eccentric but decays as a result of drag. Much inspiration is taken from the research here in order to formulate relative motion models that implement drag perturbations that are quadratic in velocity.

This paper is organized as follows, Section 2 presents the theoretical formulation of the equations of relative motion that incorporates the effect of the J_2 perturbation and quadratic drag. The analysis of the newly developed relative motion model compared to the simplistic Hill's equations and studies in Section 3, this section illuminates more on the effect of J_2 and drag on the relative motion, and justifies the importance

of its implementation in a linear model for the study of rendezvous trajectories. The set up of the optimization problem is presented in Section 4 and the results are presented and analyzed in Section 5.

2. RELATIVE MOTION MODELS

Figure 1 illustrates the curvilinear \hat{x} (radial) \hat{y} (along-track) \hat{z} (cross-track) axis system used for the problem. The \hat{x} vector points in the radial direction, the \hat{z} vector is perpendicular to the orbital plane and points in the direction of the angular momentum vector. Finally, the \hat{y} vector completes movement. In the \hat{x} - \hat{y} - \hat{z} coordinate system, the specification is made that it is a curvilinear coordinate system. The \hat{x} vector remains unchanged, however the \hat{y} and the \hat{z} vector 'curves' around the orbit.

Unlike the Local Vertical, Local Horizontal (LVLH) body fixed frame, implemented by the Hill's equations, the only difference comes from the fact that the LVLH frame is not defined as a curvilinear system but as a rectangular.

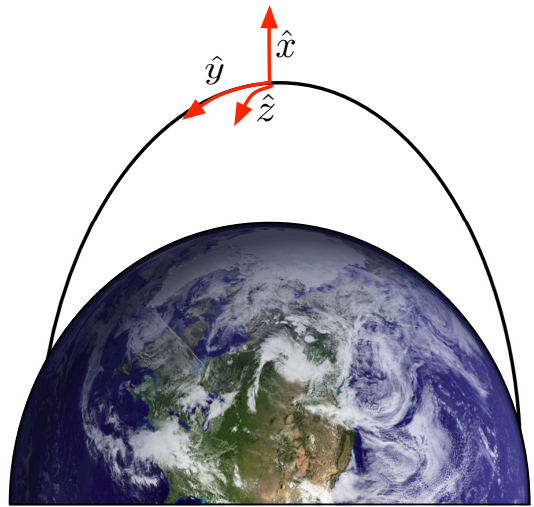


Figure 1. The \hat{x} - \hat{y} - \hat{z} Curvilinear Body-Fixed Coordinate System.

Figure 2 illustrates the \hat{r} - $\hat{\theta}$ - \hat{i} spherical coordinate system used to describe the gravitational acceleration and the J_2 potential due to the spherical earth. The \hat{r} points in the radial direction, \hat{i} is the azimuthal angle measured around the line of nodes, and $\hat{\theta}$ is the co-latitude measured from the ascending node which acts as the "pole" of the spherical system.

Conversion between both these body fixed coordinate systems is fairly straightforward. The radial vector in each coordinate system completely coincides. The \hat{y} vector, and $\hat{\theta}$ coincide; and the \hat{z} vector and the \hat{i} vector coincide. In this way, the curvilinear coordinate system defined is very much like a spherical coordinate system.

A summary of the mathematical model development is performed and described below in order to highlight the set of equations of motion that are considered for the relative motion problem between a controlled satellite (Chaser) w.r.t to the assumed reference orbit (Non-Cooperative Target).

To derive a fully linearized relative equations of motion

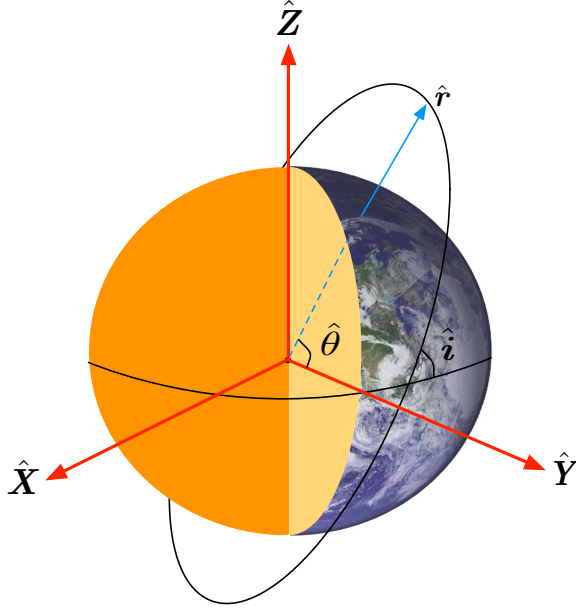


Figure 2. The \hat{r} - $\hat{\theta}$ - \hat{i} Spherical Body-Fixed Coordinate System.

that capture the J_2 perturbation with all the corrections as described by Patel and Udrea [13], along with capturing the quadratic drag disturbances, we start with formalizing the equations of motion of the secondary spacecraft under these perturbations. In the inertial frame discussed above, the equation of motion of the secondary (deputy/chaser) spacecraft is given by,

$$\ddot{\mathbf{r}} = \mathbf{g}(\mathbf{r}) + \mathbf{J}_2(\mathbf{r}) + \mathbf{f}_{\text{drag}}(\mathbf{r}) \quad (1)$$

where, $\mathbf{g}(\mathbf{r})$ is the gravitational acceleration due to spherical Earth,

$$\mathbf{g}(\mathbf{r}) = -(\mu/r^2)\hat{\mathbf{r}} \quad (2)$$

$\mathbf{J}_2(\mathbf{r})$ is the acceleration due to the J_2 potential [14],

$$\mathbf{J}_2(\mathbf{r}) = -(3/2)(J_2\mu R_e^2/r^4) \begin{bmatrix} (1 - 3 \sin^2 i \sin^2 \theta) \\ (2 \sin^2 i \sin \theta \cos \theta) \\ (2 \sin i \cos i \sin \theta) \end{bmatrix}^T \cdot [\hat{\mathbf{x}} \quad \hat{\mathbf{y}} \quad \hat{\mathbf{z}}]^T \quad (3)$$

\mathbf{r} is the position vector of the satellite, and $\hat{\mathbf{x}}\hat{\mathbf{y}}\hat{\mathbf{z}}$ is the coordinate system described in Figure 1.

$$\mathbf{f}_{\text{drag}}(\mathbf{r}) = -\beta f(r)|\dot{\mathbf{r}}|\dot{\mathbf{r}} = -\beta \frac{1}{r} |\dot{\mathbf{r}}|\dot{\mathbf{r}} \quad (4)$$

finally $\mathbf{f}_{\text{drag}}(\mathbf{r})$ is the acceleration due to drag, quadratic in velocity [8]. Here, β is a physical constant associated with the drag coefficient and the geometry of the spacecraft. The function $f(r)$ represents atmospheric density and is assumed

to only depend on altitude, its dependence on other variables like longitude, latitude, solar cycle are not considered. As \mathbf{r} represents the position of the reference spacecraft in the inertial frame, $\dot{\mathbf{r}}$ is the velocity of the spacecraft such that $|\dot{\mathbf{r}}| = (\dot{\mathbf{r}} \cdot \dot{\mathbf{r}})^{1/2}$. The function $f(r) = 1/r$ here naively models the atmospheric density using an approximate inverse law model.

The models are developed by considering the relative motion between one satellite and a reference orbit. The relative position of the satellite with respect to the reference orbit is given by \mathbf{x} as represented in Figure 3

$$\mathbf{x} = \mathbf{r} - \mathbf{r}_{\text{ref}} \quad (5)$$

Substituting $\mathbf{r} = \mathbf{r}_{\text{ref}} + \mathbf{x}$ in Equation (1),

$$\ddot{\mathbf{r}} = \ddot{\mathbf{r}}_{\text{ref}} + \ddot{\mathbf{x}} = \mathbf{g}(\mathbf{r}_{\text{ref}} + \mathbf{x}) + \mathbf{J}_2(\mathbf{r}_{\text{ref}} + \mathbf{x}) + \mathbf{f}_{\text{drag}}(\mathbf{r}_{\text{ref}} + \mathbf{x}) \quad (6)$$

In order to not lose the effect of drag constant parameter for the secondary spacecraft β while undergoing the linearization through series expansion, the drag acceleration definition in the above equation is modified such that,

$$\ddot{\mathbf{r}} = \ddot{\mathbf{r}}_{\text{ref}} + \ddot{\mathbf{x}} = \mathbf{g}(\mathbf{r}_{\text{ref}} + \mathbf{x}) + \mathbf{J}_2(\mathbf{r}_{\text{ref}} + \mathbf{x}) + \beta \mathbf{f}_{\text{drag}}(\mathbf{r}_{\text{ref}} + \mathbf{x}) \quad (7)$$

Here $\mathbf{f}_{\text{drag}}(\mathbf{r}) = \beta \mathbf{f}_{\text{drag}}(\mathbf{r})$ from modifying Equation (4). In order to linearize the above equation, the vectors $\mathbf{g}(\cdot)$, $\mathbf{J}_2(\cdot)$ and $\mathbf{f}_{\text{drag}}(\cdot)$ are expanded in a Taylor's series about the reference spacecraft \mathbf{r}_{ref} , which gives,

$$\mathbf{g}(\mathbf{r}_{\text{ref}} + \mathbf{x}) = \mathbf{g}(\mathbf{r}_{\text{ref}}) + \nabla \mathbf{g}(\mathbf{r}_{\text{ref}}) \mathbf{x} + \mathcal{O}^N \quad (8)$$

$$\mathbf{J}_2(\mathbf{r}_{\text{ref}} + \mathbf{x}) = \mathbf{J}_2(\mathbf{r}_{\text{ref}}) + \nabla \mathbf{J}_2(\mathbf{r}_{\text{ref}}) \mathbf{x} + \mathcal{O}^N \quad (9)$$

Because the vector function $\mathbf{f}_{\text{drag}}(\mathbf{r}_{\text{ref}} + \mathbf{x})$ which depends on the derivative of the linearized quantity $\dot{\mathbf{r}}_{\text{ref}}$ at which its expanded upon. Converting the vector function so it depends only in the position, gives

$$\begin{aligned} \mathbf{f}_{\text{drag}}(\mathbf{r}_{\text{ref}} + \mathbf{x}) &= \underbrace{f(r_{\text{ref}})\dot{r}_{\text{ref}}\dot{\mathbf{r}}_{\text{ref}} + f(r_{\text{ref}})\dot{r}_{\text{ref}}\dot{\mathbf{x}}}_{f_{\text{drag}}(\mathbf{r}_{\text{ref}})} \\ &+ f(r_{\text{ref}})\dot{r}_{\text{ref}} \left[\frac{\mathbf{r}_{\text{ref}} \cdot \mathbf{x}}{r_{\text{ref}}^2} \right] \dot{\mathbf{r}}_{\text{ref}} \\ &+ f'(r_{\text{ref}}) \left[\frac{\mathbf{r}_{\text{ref}} \cdot \mathbf{x}}{r_{\text{ref}}} \right] \dot{\mathbf{r}}_{\text{ref}} \\ &+ \mathcal{O} \left[\frac{\mathbf{r}_{\text{ref}} \cdot \mathbf{x}}{\nabla \nabla \mathbf{f}_{\text{drag}}} \right] \end{aligned} \quad (10)$$

Here $f(r) = -1/r$ the simplistic density modeling function as seen in Equation (4) with the negative sign carried inside. Ignoring all the second- and higher-order terms under the assumption that for a relative position $|\mathbf{x}|/|\mathbf{r}_{\text{ref}}| \ll 1$, and substituting the above set of Equations (9) (10) and (11) into Equation (8), gives,

$$\nabla \mathbf{J}_2(\mathbf{r}) = \frac{6\mu J_2 R_e^2}{r^5} \begin{bmatrix} (1 - 3 \sin^2 i \sin^2 \theta) & \sin^2 i \sin 2\theta & \sin 2i \sin 2\theta \\ \sin^2 i \sin 2\theta & -\frac{1}{2} - \sin^2 i (\frac{1}{2} - \frac{7}{4} \sin^2 \theta) & -\frac{\sin 2i \cos \theta}{4} \\ \sin 2i \sin \theta & -\frac{\sin 2i \cos \theta}{4} & -\frac{3}{4} + \sin^2 i (\frac{1}{2} + \frac{5}{4} \sin^2 \theta) \end{bmatrix} \quad (14)$$

$$\begin{aligned} \ddot{\mathbf{x}} = & \mathbf{g}(\mathbf{r}_{\text{ref}}) + \nabla \mathbf{g}(\mathbf{r}_{\text{ref}}) \cdot \mathbf{x} + \mathbf{J}_2(\mathbf{r}_{\text{ref}}) + \nabla \mathbf{J}_2(\mathbf{r}_{\text{ref}}) \cdot \mathbf{x} \\ & + \beta f_{\text{drag}}(\mathbf{r}_{\text{ref}}) + \beta f_{\text{drag}}(\mathbf{r}_{\text{ref}}) \left[\frac{\mathbf{r}_{\text{ref}} \cdot \mathbf{x}}{r_{\text{ref}}^2} \right] \\ & + \beta f(r_{\text{ref}}) \dot{r}_{\text{ref}} \dot{\mathbf{x}} + \beta f'(r_{\text{ref}}) \left[\frac{\mathbf{r}_{\text{ref}} \cdot \mathbf{x}}{r_{\text{ref}}} \right] \dot{\mathbf{r}}_{\text{ref}} - \ddot{\mathbf{r}}_{\text{ref}} \end{aligned} \quad (11)$$

$$\begin{aligned} \ddot{\mathbf{x}}^{\mathcal{T}} = & \nabla \mathbf{g}(\mathbf{r}_{\text{ref}}) \cdot \mathbf{x} + \mathbf{J}_2(\mathbf{r}_{\text{ref}}) + \nabla \mathbf{J}_2(\mathbf{r}_{\text{ref}}) \cdot \mathbf{x} \\ & + (\beta - \alpha) f_{\text{drag}}(\mathbf{r}_{\text{ref}}) + \beta f_{\text{drag}}(\mathbf{r}_{\text{ref}}) \left[\frac{\mathbf{r}_{\text{ref}} \cdot \mathbf{x}}{r_{\text{ref}}^2} \right] \\ & + \beta f(r_{\text{ref}}) \dot{r}_{\text{ref}} \dot{\mathbf{x}} + \beta f'(r_{\text{ref}}) \left[\frac{\mathbf{r}_{\text{ref}} \cdot \mathbf{x}}{r_{\text{ref}}} \right] \dot{\mathbf{r}}_{\text{ref}} \\ & - \frac{1}{2\pi} \int_0^{2\pi} \mathbf{J}_2(\mathbf{r}_{\text{ref}}) d\theta - [\mathbf{J}_2(\mathbf{r}_{\text{ref}}) \cdot \hat{\mathbf{z}}] \hat{\mathbf{z}} \end{aligned} \quad (13)$$

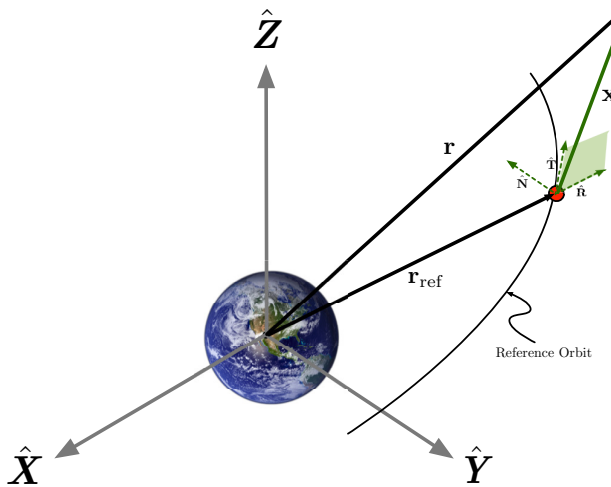


Figure 3. The Reference Orbit

Similar to Equation (1), the inertial acceleration of the primary/deputy spacecraft placed in the reference orbit can be written as,

$$\begin{aligned} \ddot{\mathbf{r}}_{\text{ref}} = & \mathbf{g}(\mathbf{r}_{\text{ref}}) + \underbrace{\frac{1}{2\pi} \int_0^{2\pi} \mathbf{J}_2(\mathbf{r}_{\text{ref}}) d\theta}_{\text{Period Correction}} + \underbrace{[\mathbf{J}_2(\mathbf{r}_{\text{ref}}) \cdot \hat{\mathbf{z}}] \hat{\mathbf{z}}}_{\text{Drift Correction}} \\ & + \alpha f_{\text{drag}}(\mathbf{r}_{\text{ref}}) \end{aligned} \quad (12)$$

Here, α similar to β depends on the drag coefficient and the geometrical parameters of the primary spacecraft. The correction terms comes about the derivation as formulated previously by Patel and Udrea [13] and the drag acceleration uses the modified definition with α being the drag constant for the primary spacecraft.

Substituting Equation (12) in (1) and canceling out the $\mathbf{g}(\mathbf{r}_{\text{ref}})$ term, gives,

For the gradient of the vector functions in the above expression, when a spherical coordinate system ($\hat{\mathbf{r}} - \hat{\theta} - \hat{\mathbf{i}}$) with the pole aligned with the ascending node is used, the gradient of the $\mathbf{g}(\mathbf{r})$ gravitational acceleration can be calculated. The result is:

$$\nabla \mathbf{g}(\mathbf{r}) = \begin{bmatrix} 2(\mu/r^3) & 0 & 0 \\ 0 & -(\mu/r^3) & 0 \\ 0 & 0 & -(\mu/r^3) \end{bmatrix} \quad (14)$$

The \mathbf{J}_2 disturbance in Equation (3) is given in $\hat{\mathbf{x}} - \hat{\mathbf{y}} - \hat{\mathbf{z}}$ coordinates. However, the equation can be transformed directly to the $\hat{\mathbf{r}} - \hat{\theta} - \hat{\mathbf{i}}$ coordinate system without any loss of generality. Taking the gradient gives Equation (8)

Because the reference frame is rotating, rotational terms are added when calculating the relative acceleration and velocity of the satellite w.r.t. the reference orbit. The relative motion above can now be converted into the rotating frame using the transport theorem.

$$\ddot{\mathbf{x}}^{\mathcal{T}} = \ddot{\mathbf{x}}^{\mathcal{R}} + 2\omega^{\mathcal{R}} \times \dot{\mathbf{x}}^{\mathcal{R}} + \dot{\omega}^{\mathcal{R}} \times \mathbf{x}^{\mathcal{R}} + \omega^{\mathcal{R}} \times (\omega^{\mathcal{R}} \times \mathbf{x}^{\mathcal{R}}) \quad (15)$$

Substituting Equation (13) into (15) and correcting for the derivatives on the RHS gives,

$$\begin{aligned} \ddot{\mathbf{x}}^{\mathcal{R}} + 2\omega^{\mathcal{R}} \times \dot{\mathbf{x}}^{\mathcal{R}} + \dot{\omega}^{\mathcal{R}} \times \mathbf{x}^{\mathcal{R}} + \omega^{\mathcal{R}} \times (\omega^{\mathcal{R}} \times \mathbf{x}^{\mathcal{R}}) = & \nabla \mathbf{g}(\mathbf{r}_{\text{ref}}) \cdot \mathbf{x} + \mathbf{J}_2(\mathbf{r}_{\text{ref}}) + \nabla \mathbf{J}_2(\mathbf{r}_{\text{ref}}) \cdot \mathbf{x} + (\beta - \alpha) f_{\text{drag}}(\mathbf{r}_{\text{ref}}) \\ & + \beta f_{\text{drag}}(\mathbf{r}_{\text{ref}}) \left[\frac{\mathbf{r}_{\text{ref}} \cdot \mathbf{x}}{r_{\text{ref}}^2} \right] + \beta f(r_{\text{ref}}) \dot{r}_{\text{ref}} (\dot{\mathbf{x}} + \omega^{\mathcal{R}} \times \mathbf{x}) \\ & + \beta f'(r_{\text{ref}}) \left[\frac{\mathbf{r}_{\text{ref}} \cdot \mathbf{x}}{r_{\text{ref}}} \right] (\dot{\mathbf{r}}_{\text{ref}} + \omega^{\mathcal{R}} \times \mathbf{r}_{\text{ref}}) \\ & - \frac{1}{2\pi} \int_0^{2\pi} \mathbf{J}_2(\mathbf{r}_{\text{ref}}) d\theta - [\mathbf{J}_2(\mathbf{r}_{\text{ref}}) \cdot \hat{\mathbf{z}}] \hat{\mathbf{z}} \end{aligned} \quad (16)$$

The above now represents linear differential equation that describes the motion of the secondary spacecraft with respect to the target spacecraft (reference orbit). The equation still encompasses some time varying coefficients. The problem comes about that $\nabla \mathbf{J}_2$ term is not going to be constant except for equatorial orbits, where the effect of J_2 perturbation is negligible. A solution to this problem is to approximate the gradient of J_2 with the average value of the gradient term as a function of inclination for an entire period. Below is the approximate value of time average $\nabla \mathbf{J}_2$ term.

$$\nabla \mathbf{J}_2(\mathbf{r}) \approx \frac{1}{2\pi} \int_0^{2\pi} \nabla \mathbf{J}_2(\mathbf{r}) d\theta = \frac{\mu}{r^3} \begin{bmatrix} 4s & 0 & 0 \\ 0 & -s & 0 \\ 0 & 0 & -3s \end{bmatrix} \quad (17)$$

here s is given by,

$$s = \frac{3J_2R_e^2}{8r^2}(1 + 3 \cos 2i) \quad (18)$$

The period correction term in Equation (16) is essentially the average J_2 disturbance over one period (not to be confused with the time average of the gradient of the J_2 term discussed above). This result of averaging J_2 for a period is a non-zero value for acceleration in the radial \hat{x} direction only as shown below in Equation (19). This can be visualized as an additional force acting to increase the Keplerian gravity term. Therefore, if a satellite is to remain in a circular orbit its orbital rate must be increased above that for Keplerian dynamics.

$$\frac{1}{2\pi} \int_0^{2\pi} \mathbf{J}_2(\mathbf{r}) d\theta = \begin{bmatrix} -n^2rs \\ 0 \\ 0 \end{bmatrix} \quad (19)$$

here s is same as described in Equation (18). Detail derivation of the corrections and analysis on the effect of averaging J_2 potential and its gradients are discussed in Patel and Udrea [13].

With the substitutions for the gradient, and the time average J_2 the above Equation (16) with time-varying terms can now be written out in its vector components form as follow,

$$\begin{aligned} \ddot{x} &= 2\omega\dot{y} + (5c^2 - 2)n^2x \\ &- \frac{3n^2J_2R_e^2}{r_{ref}} \left[\frac{1}{2} - \frac{3 \sin^2 i_{ref} \sin^2(kt)}{2} - \frac{1 + \cos 2i_{ref}}{8} \right] \\ &- (\beta - \alpha) \left[-\omega^2y + \omega\dot{x} + \left(\frac{\dot{r}_{ref}}{r_{ref}} \right) \omega x + h^{-\frac{1}{2}}r_{ref}\dot{r}_{ref}e^{\alpha\theta} \right] \\ \ddot{y} &= -2\omega\dot{x} - \frac{3n^2J_2R_e^2}{2r_{ref}} [\sin^2 i_{ref} \sin(2kt)] \\ &+ (\beta - \alpha) \left[-\omega^2x - \omega\dot{y} - \left(\frac{\dot{r}_{ref}}{r_{ref}} \right) \omega y - h^{-\frac{1}{2}}r_{ref}^2e^{\alpha\theta}\omega^2 \right] \\ \ddot{z} &= -(3c^2 - 2)n^2z - (\beta - \alpha) \left[\omega\dot{z} + \left(\frac{\dot{r}_{ref}}{r_{ref}} \right) \omega z \right] \end{aligned} \quad (20)$$

where k is given below with $J_2 = 1.081875 \times 10^{-3}$ [20],

$$k = \underbrace{n\sqrt{1+s}e^{-\alpha\theta}}_{\omega} + \frac{3\sqrt{\mu J_2 R_e^2}}{2r_{ref}^{7/2}} \cos^2 i \quad (21)$$

The angular velocity of the reference orbit which was assumed to be constant initially is corrected to incorporate the period correction due to the added J_2 perturbation, additionally there will also be a decay term associated with the angular velocity due to the drag perturbation as shown below,

$$\omega = n\sqrt{1+s} e^{-\alpha\theta} \quad s = \frac{3J_2R_e^2}{8r^2}(1 + 3 \cos 2i) \quad (22)$$

The above transformation from Equation (16) to (20) is made possible by the close form solution developed by Carter and Humi [8] that describes the motion of the reference spacecraft under quadratic drag. The solution gives an orbit degradation equation of a spacecraft which is initially elliptical but not highly eccentric. r_{ref} in the above Equation (20) will be given by this solution,

$$r_{ref} = \frac{h^2(1 + 4\alpha^2)/\mu}{e^{2\alpha\theta} + \epsilon_0 \cos(\theta - \theta_0)} \quad (23)$$

Differentiating the above equation with respect to time, we get

$$\dot{r}_{ref} = \frac{-(h^2(1 + 4\alpha^2)/\mu) \cdot (e^{2\alpha\theta} 2\alpha\omega - \epsilon_0 \omega \sin(\theta - \theta_0))}{(e^{2\alpha\theta} + \epsilon_0 \cos(\theta - \theta_0))^2} \quad (24)$$

with ω as the angular velocity of the rotating coordinate system which is corrected in the presence of drag and J_2 disturbance. The theoretical formulation of ω is shown in Equation (22). h is the angular momentum that comes about as the constant of integral when deriving the orbit equation as described in Equation (23). While, ϵ_0 and θ_0 represents the initial eccentricity and the initial true anomaly of the reference orbit respectively.

The above equations in all its entirety now facilitates the study of the relative motion of two space crafts under a high fidelity perturbation model which includes both time-averaged J_2 with corrections and quadratic drag. This model is the foundation for the control problem implemented in the later chapter. Although this model is a vast improvement over Hill's equations of motion, a better approximation would be improving on the density modeling function $f(r)$, the current density variation is captured by the inverse law which can be improved upon by considering atmospheric density decay that is exponential with an increase in r . Moreover, a parametric curve fit on the standard atmospheric data could also be considered. The difficulty with more realistic density models is to be able to find any close form solutions.

Next Section shows the importance of implementing these disturbances by propagating orbits in time for different criteria, magnitude of error in relative position and velocity between different models will show the influence of these perturbations. Moreover, physics of the above formulated model is verified by simulating trajectories at 0° inclination compared to Hill's model, similar behavior is expected in relative position and velocity.

3. EFFECTS OF PERTURBATIONS

This section highlights the effects of J_2 and quadratic drag perturbations on the relative motion of the perturbed satellite with respect to the reference orbit. This is done to facilitate and show the importance of the implemented perturbations and to make a better dynamical constraint for different control schemes that are studied later in the paper.

Numerical simulations are performed using fixed-step ODE5 integrator to plot relative motion trajectories. The orbital parameters chosen for the reference orbit where the target is placed are: $i_{\text{ref}} = 70^\circ$, the apogee and perigee altitude is given by $r_a = 919\text{-km}$ and $r_p = 902\text{-km}$ respectively. The rationale for choosing the above orbital parameters is discussed in Sec. 4 where the optimization problem for this study is formulated.

Effect of J_2 Disturbance

The following Figure 4 demonstrates the effect of the J_2 geopotential disturbances at 70° inclination. The purpose to acquire the J_2 effect on the chaser from both the equatorial and polar regions, a logical choice of starting from $[-1, 0, 0]$ km is employed as the initial condition for the relative position, thus in order to attempt to only simulate the J_2 effect on the pure in-track motion. The chaser is assumed to be at rest initially. All the simulations below for this section are propagated for the time span of two orbital period of the reference orbit which comes to 3.44 hrs.

It is seen in Figure 4 the considerable relative position error created by the J_2 disturbance and the importance for its implementation while studying the optimal trajectory design for rendezvous and proximity operations. Additionally, it is noted that the J_2 model without corrections adds sizable cross-track errors as a result of orbital period mismatch between the target and the chaser orbits and, the nodal drift caused by the separation of the longitude of the ascending node.

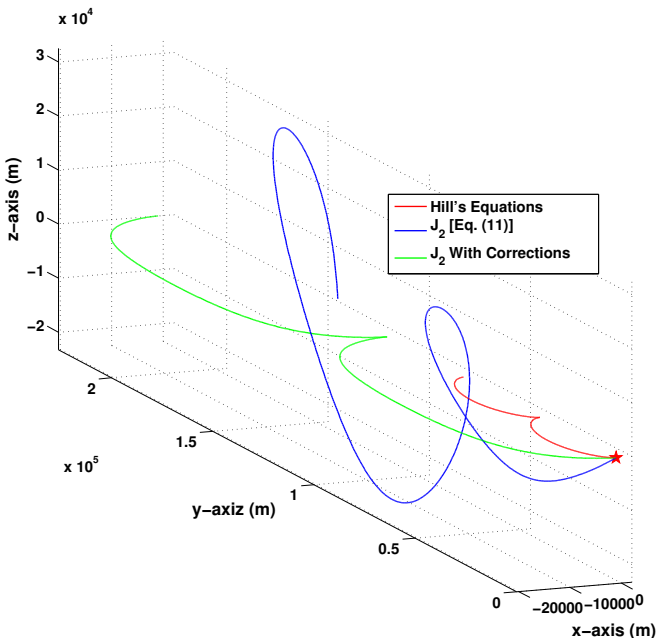


Figure 4. Relative motion trajectories ($i_{\text{ref}} = 70^\circ$).

The relative position errors between the commonly used

Hill's equations and the time-averaged J_2 with corrections model is shown in Figure 5. As seen in the figure, the error in the in-track motion (\hat{x}) tops out at ~ 15 km and error propagation in time looks periodic. Similarly, for the radial motion (\hat{y}) the error due to the J_2 seems to be increasing sharply with time. Finally, for the cross-track motion (\hat{z}) even though the error is not significant compared to in-track and radial motion, the profile shows an increasing deviation with time. With periodic errors in the in-track motion and the increasing errors in both the radial and cross-track direction, a significant effect of J_2 perturbation on the chaser is seen.

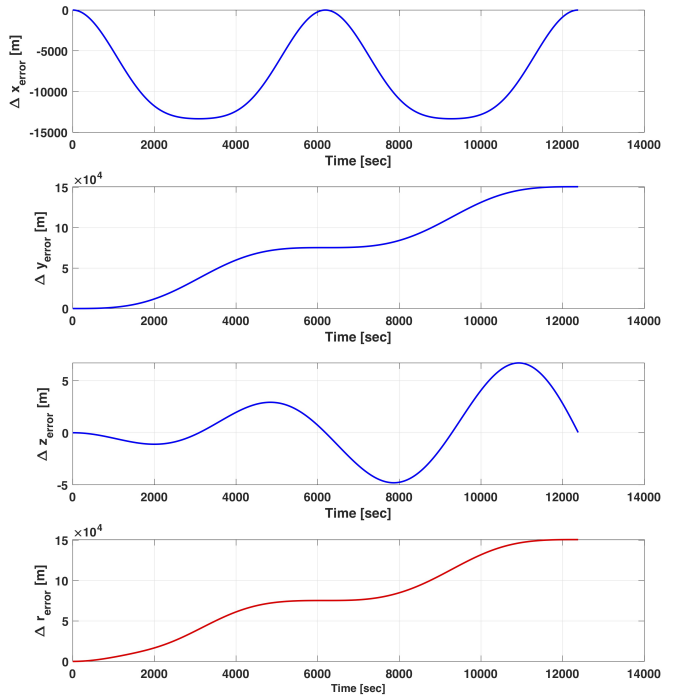


Figure 5. Relative position errors between Hill's Eqns. and Time-averaged J_2 with corrections Eqns. ($i_{\text{ref}} = 70^\circ$).

Figure 6 presents similar relative position errors between the time-averaged J_2 model with corrections and, the J_2 equations without any corrections to highlight the effect caused by the orbital period mismatch and the separation in the ascending node causing the nodal drift. As expected, the position error in all three directions is significant. As a consequence, the implementation of the corrections is crucial for studying the optimal trajectory design for proximity applications. Moreover when compared to Figure 5, it is seen that the implementation of the corrections reduces error in the \hat{z} direction which causes the motion of the chaser to create heavy cross-track deviations from the nominal as seen in Figure 4.

One way to validate the physics of the newly developed linearized model is to analyze it at 0° inclination. As the effect of J_2 is not prominent on the equatorial plane, the time-averaged J_2 with corrections model should behave similar to Hill's equations of motion. Figure 7 shows the relative motion trajectories under the influence of the J_2 disturbance force. It is seen that the relative motion of the chaser under the time-averaged J_2 with corrections model resembles with that of Hill's equations, as logically there would not be any effect of J_2 across the equator. Although a significant error is seen in the relative position given by the J_2 equations without corrections.

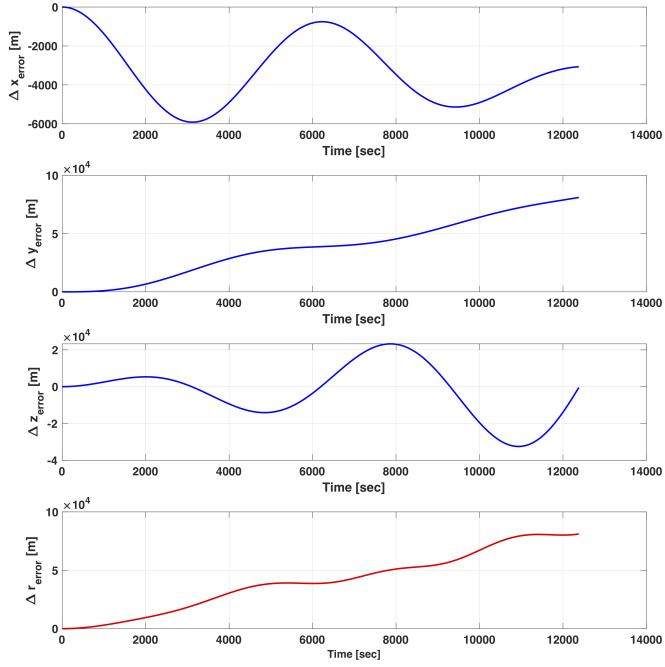


Figure 6. Relative position errors between Time-averaged J_2 with corrections Eqns. and J_2 without corrections Eqns. [Eqn. (11)] ($i_{\text{ref}} = 70^\circ$).

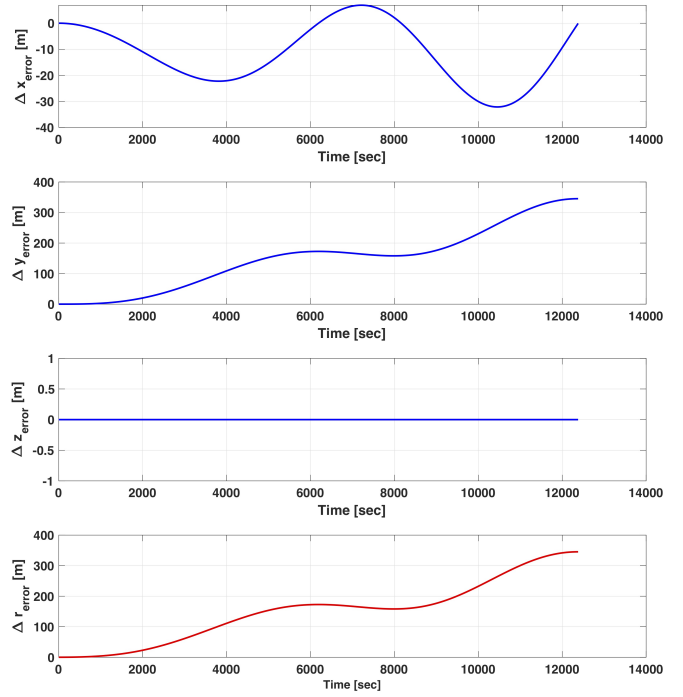


Figure 8. Relative position errors between Hill's Eqns. and Time-averaged J_2 with corrections Eqns. ($i_{\text{ref}} = 0^\circ$).

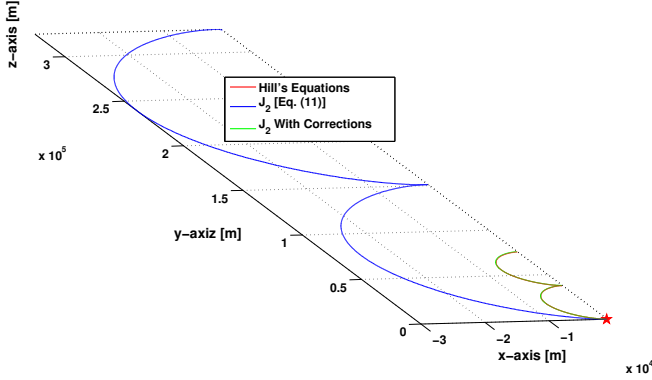


Figure 7. Relative motion trajectories ($i_{\text{ref}} = 0^\circ$).

Figure 8 illustrates the errors in the relative position of the spacecrafts between time-averaged J_2 with corrections model and Hill's Equations.

Figure 8 shows that the position errors between J_2 corrections model with Hill's equation are very small. The insignificant error noticed corresponds to errors due to linearization. We see the error in the radial direction (\hat{y}) has secular growth, for higher period orbits the linearization breaks down as $\mathbf{r}_{\text{ref}} \gg \mathbf{x}$ is no longer a valid condition. Validating the time-averaged J_2 corrections model at 0° inclination proves that the model used for the optimization problem in the following section is a generalized case of Hill's Equation with J_2 perturbation incorporated in it.

From the study conducted in this section we see the importance of implementation of J_2 in the linear equations of relative motion for the study of the optimization operations.

Effect of Quadratic Drag Disturbance

While implementing drag effect it is crucial to define the geometric parameters for both the spacecraft, we start with assuming the secondary spacecraft (chaser) with a mass of $m_{\text{chaser}} = 24\text{-kg}$ and surface area of $A_{\text{chaser}} = 0.23 \times 0.23 = 0.0526\text{-m}^2$. The rational about this assumption is discussed in detail under Chapter [4] where the control problem is formulated. As discussed previously, the reference space object is assumed to a upper stage debris Agena-D, the dry mass for this upper stage is given as $m_{\text{ref}} = 673\text{-kgs}$ with the cross section area of $A_{\text{ref}} = 1.5 \times 6.5 = 9.75\text{-m}^2$ [19]. The ballistic coefficient can now be calculated and given below in Equation (25).

$$\beta_{\text{chaser}} = \frac{0.0526 \times 10^{-6}}{24} = 2.204 \times 10^{-8}\text{km}^2/\text{kg}$$

$$\beta_{\text{ref}} = \frac{9.75 \times 10^{-6}}{673} = 1.449 \times 10^{-7}\text{km}^2/\text{kg} \quad (25)$$

From the ballistic coefficients it can be noted that the reference space object is almost $\times 6.57$ bigger than the secondary spacecraft. Section below further expands by studying the influence of drag for a system of two spacecraft with higher ballistic coefficient ratios. To simulate the most extreme scenario, the drag coefficient of $C_d = 2.1$ is used, this implies both the spacecrafts being flat plates and are aligned perpendicular exposing their full area in the direction of motion.

The secondary spacecraft is assumed to be at rest initially and starting at $[-1, 0, 0]$ km. All simulations below for this subsection are propagated for the time span of two orbital periods of the reference orbit which comes to 3.44 hrs.

Figure 9 below highlights the effect of Quadratic drag perturbation at an altitude of 911-km. As seen the relative position and velocity errors between the drag model and Hill's equation of motion are fairly noticeable. It is expected that the magnitude in error when compared to J_2 model with corrections from the above subsection will be less significant, as the effect of J_2 disturbance relative to drag is highly dominant.

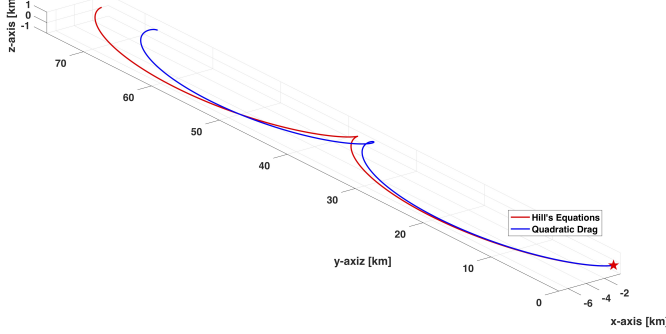


Figure 9. Relative motion trajectories at 900-km altitude with $i_{\text{ref}} = 70^\circ$ for 2-orbital period

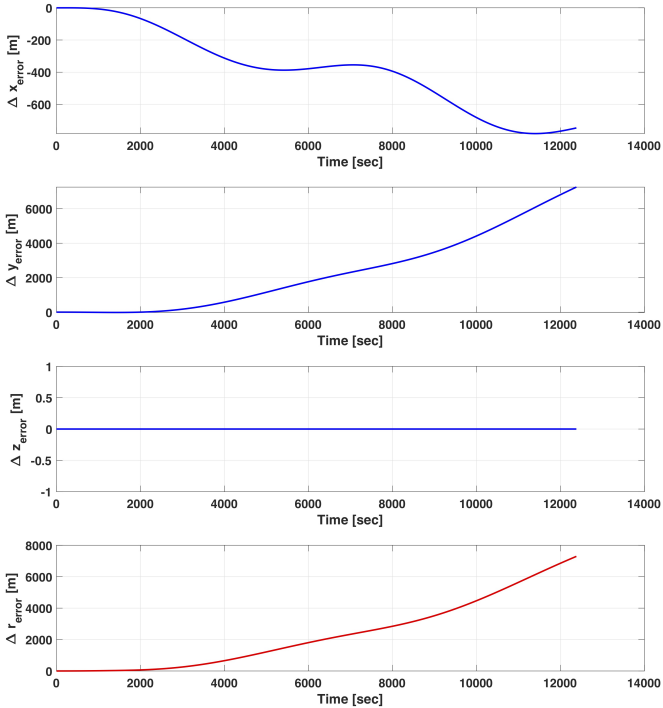


Figure 10. Relative position errors between Quadratic Drag Model and Hill's Model ($i_{\text{ref}} = 70^\circ$ with 900-km Altitude for 2-orbital period)

The relative position errors between the Hill's model and the quadratic drag model is shown in Figure 10. It can be seen that the position errors in the cross-track (\hat{z}) are negligible for the initial conditions chosen. It is shown later with different initial conditions, the cross-track motion errors are in-fact significant and also periodic with secular effects that grows with time. The radial (\hat{y}) and in-track (\hat{x}) motion shows significant errors in relative position. Both seem to increase sharply with time. With relative position errors in all three motion, a significant effect of drag perturbation on the chaser is seen. Note that for the J_2 perturbation model, the relative

position by Hill's model were always understated, whereas for the quadratic drag model, the relative positions by Hill's model are exaggerated. As drag force can be characterized as a friction force action opposite on the motion of the space crafts, the above exaggerated position errors by Hill's model seem to validate that intuition.

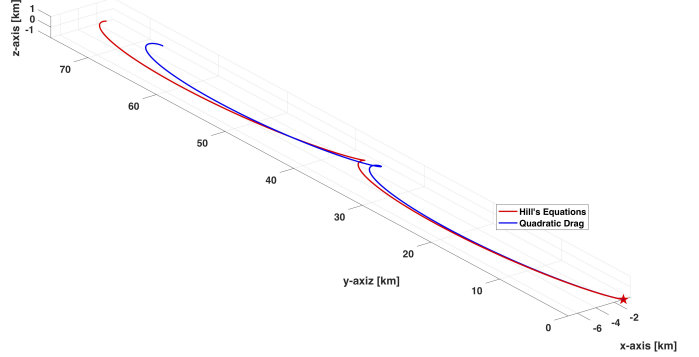


Figure 11. Relative motion trajectories - $i_{\text{ref}} = 70^\circ$ with I.C. $= [-1, 0, -1]$ for 2-orbital period (900-km altitude)

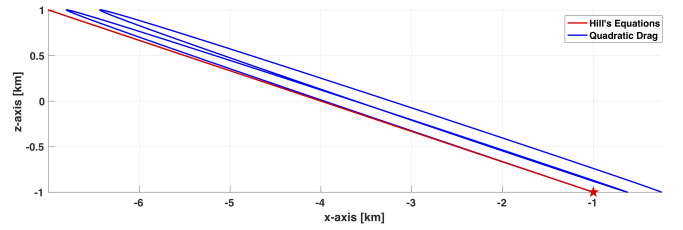


Figure 12. $\hat{x} - \hat{z}$ view for I.C. $= [-1, 0, -1]$ for 2-orbital period (900-km altitude) - Drift view

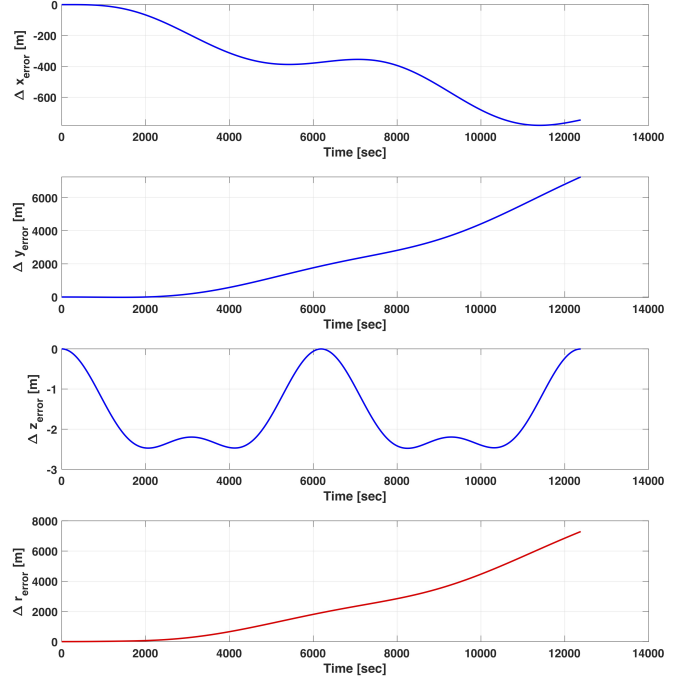


Figure 13. Relative position errors between Quadratic Drag Model and Hill's Model for I.C. $= [-1, 0, -1]$ ($i_{\text{ref}} = 70^\circ$ with 900-km Altitude for 2-orbital period)

The above Figure 11 shows the relative position errors with

change in initial conditions. The starting point for the chaser is now $[-1, 0, -1]$. This highlights the cross track (\hat{z}) motion errors. As previously stated the errors are both significant and periodic in nature.

As seen in the Figure 11 and 12, the errors in the relative motion shows significant drift contributed by the drag perturbation. These drifts also seem to increase with each orbital period of the reference orbit. Figure 13 further shows the relative position errors between the quadratic drag model and the Hill's model.

Although, as seen that the magnitude of error due to drag perturbation when compared to J_2 disturbance with corrections on relation motion are not too big, the effect of drag perturbation on the spacecraft vary on multiple factors. Hence, it facilitates a more through study of the quadratic drag model at different altitudes and for longer periods. Figure 14 and 15 shows the relative position deviations due to change in altitude. It is seen that the effect of drag gets more dominant with decrease in altitude. To highlight the periodic error prorogation in the cross track motion, the initial conditions for the secondary spacecraft are chosen as $[-1, 0, -1]$ for the figures below.

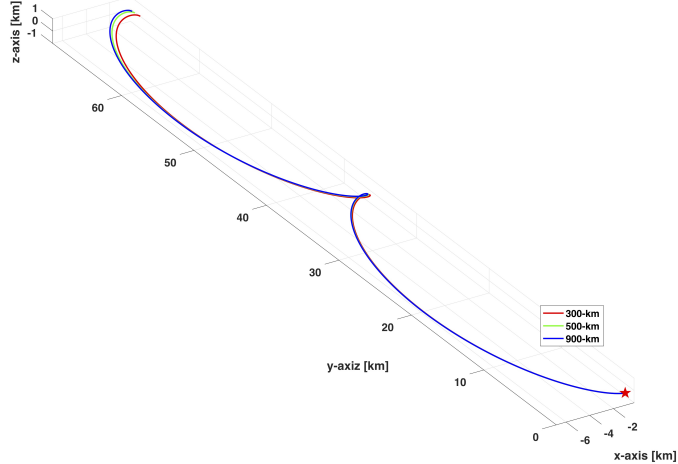


Figure 14. Relative motion trajectories with Quadratic Drag Model at multiple altitudes for I.C. = $[-1, 0, -1]$ ($i_{ref} = 70^\circ$ for 2-orbital period)

The deviations seen verifies the intuition that at lower altitudes there is a higher effect of drag perturbations. This effect is clearly highlighted in Figure 15 which zooms at the final state of the spacecrafats after 2 orbital-period. It is expected that at higher altitudes the relative position compared to lower altitudes would be exaggerated. This is purely because at higher altitudes there would be simply less drag due to lower atmospheric density. Also to note that the position deviations between lower altitudes (between 500-km and 300-km) is much higher than the position deviations between higher altitudes (between 900-km and 500-km) as shown in Figure 16. This can be again regarded to the fact that at higher altitudes the effect of drag will be much lower compared to lower altitudes.

The following Figure 17 and 18 highlights the effect of longer periods under the drag perturbation.

As discussed, the errors in relative position increase sharply with time in both radial (\hat{y}) and in-track (\hat{x}) motion, this is validated in the Figure 17, 18 and 19. When compared to

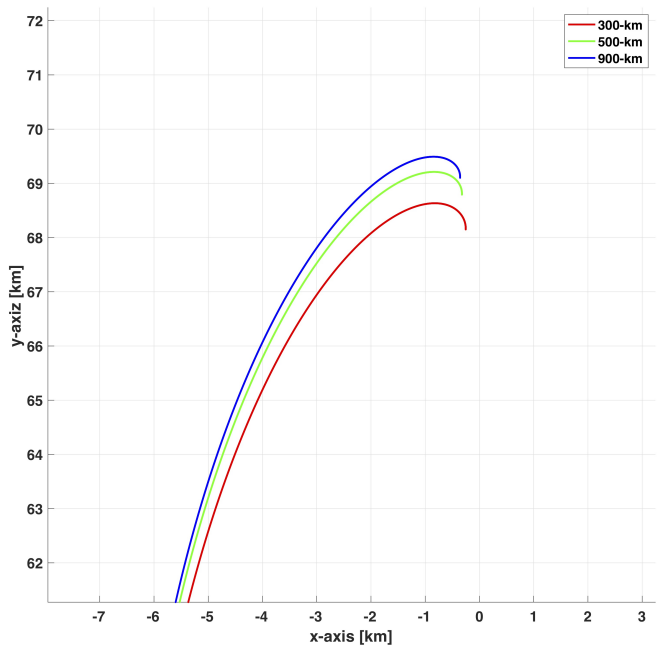


Figure 15. Zoomed view of Relative motion trajectories with Quadratic Drag Model at multiple altitudes for I.C. = $[-1, 0, -1]$ ($i_{ref} = 70^\circ$ for 2-orbital period)

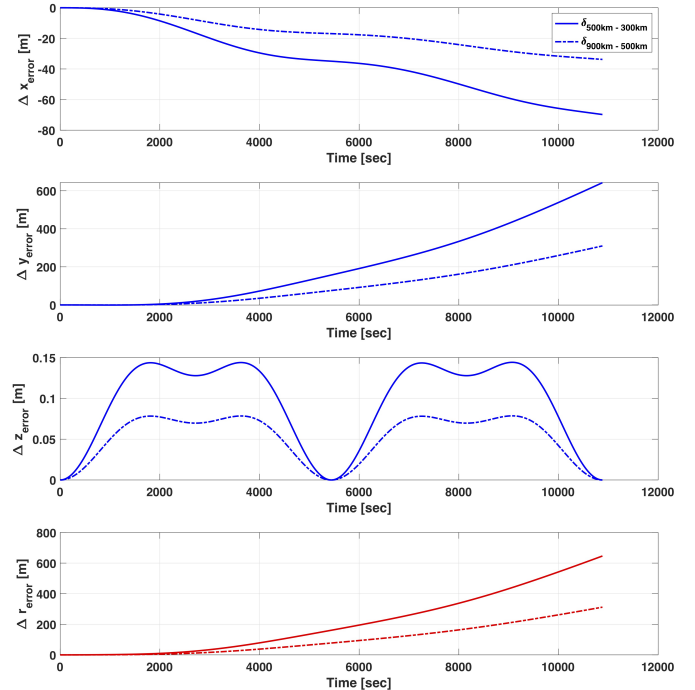


Figure 16. Relative position errors with Quadratic Drag Model for different altitudes for I.C. = $[-1, 0, -1]$ ($i_{ref} = 70^\circ$ for 2-orbital period)

Figure 12 that shows the drift for 2 orbital-period, it can be seen that for longer periods here the drift due to the drag perturbation becomes significantly prominent with time. Once again, the errors in the cross track (\hat{z}) motion are simply periodic in nature and does not have any secular growth associated with it in time. Majority of the errors in the relative position comes about the radial motion as seen in Figure 19.

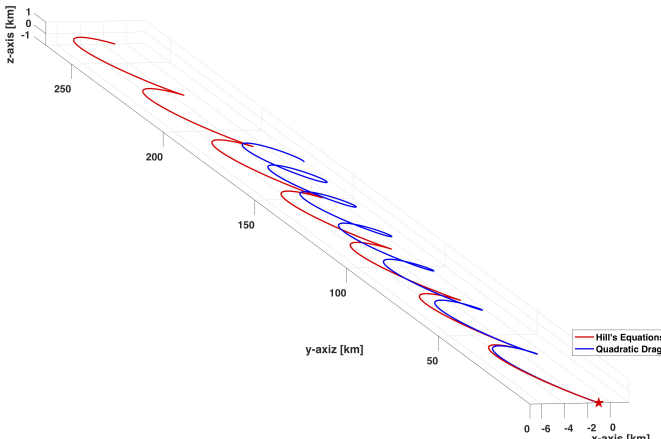


Figure 17. Relative motion trajectories - $i_{ref} = 70^\circ$ with I.C. $= [-1, 0, -1]$ for 7-orbital period (900-km altitude)

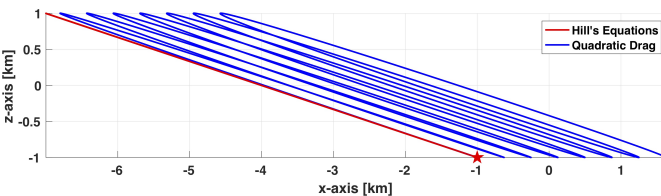


Figure 18. $\hat{x} - \hat{z}$ view for I.C. $= [-1, 0, -1]$ for 7-orbital period (900-km altitude) - Drift view

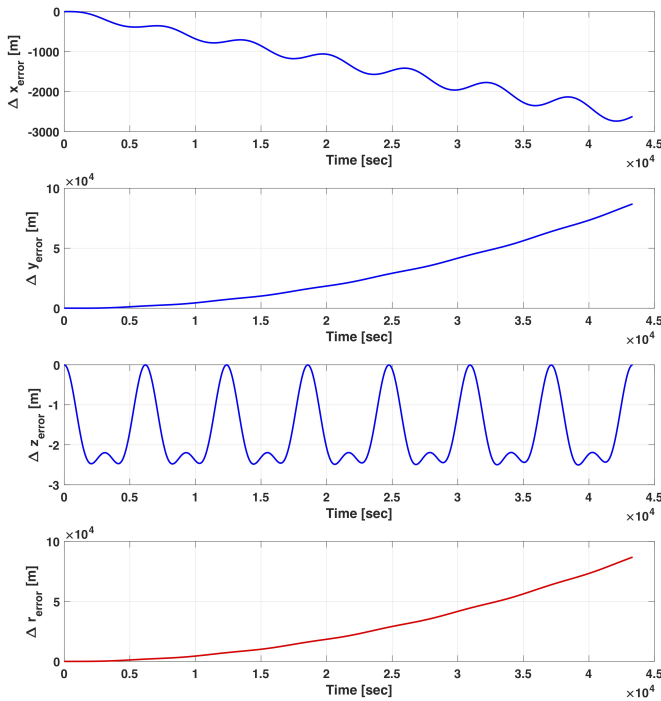


Figure 19. Relative position errors between Quadratic Drag Model and Hill's Model for I.C. $= [-1, 0, -1]$ ($i_{ref} = 70^\circ$ with 900-km Altitude for 7-orbital period)

From the study conducted in this section we see the importance of implementing quadratic drag in the linear differential equations of relative motion for the study of optimal control problems.

Similar to how the time-averaged J_2 model was validated in the above section, we can implement a similar study to cross examine the correctness of the physics in the quadratic drag model. Unlike J_2 the effect of drag does not depend on the inclination of the reference orbit, but more so on the geometrical parameters of both the spacecrafts and the altitude chosen for the reference orbit as seen above. Therefore, in order to validate the quadratic drag model, the drag constants for both the spacecrafts as defined in Equations (4) and (12) can be set to zero i.e. $\alpha = \beta = 0$. In this case, the only effect that will be pertaining to the relative position errors will be due to the fact that the Hill's models assumes a circular reference orbit. The position errors for this case are highlight in Figure 20 and 21.

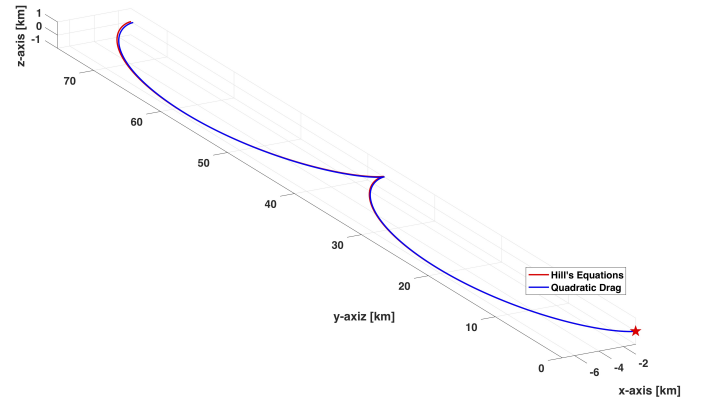


Figure 20. Relative motion trajectories for I.C. $= [-1, 0, 0]$ ($i_{ref} = 70^\circ$ with 900-km Altitude for 2-orbital period) and $\alpha = \beta = 0$

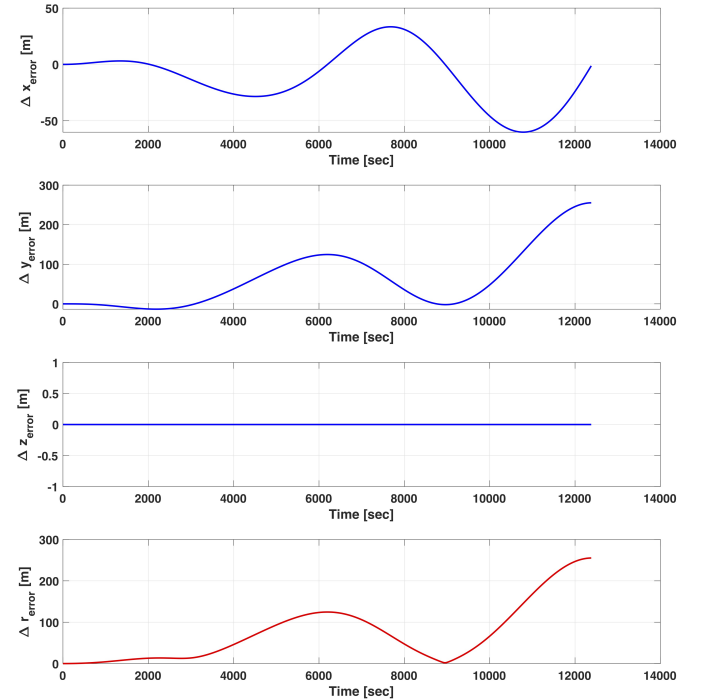


Figure 21. Relative position errors between Hill's Model and Quadratic Drag Model for I.C. $= [-1, 0, 0]$ ($i_{ref} = 70^\circ$ with 900-km Altitude for 2-orbital period) and $\alpha = \beta = 0$

As previously stated, the relative position errors seen in the above Figure 21 are caused due to the reference orbit being

eccentric. This can be validated by further setting the apogee and perigee altitude equal to each other i.e. $h_a = h_p = 902\text{-km}$. For a case like this, it is expected that the quadratic drag model should behave exactly like Hill's equations of motion for small orbital-periods. As the models formulated in the previous chapter are linearized in nature, there is a possibility that for longer periods, there will be some linearization errors that will become dominant in time. For the case with smaller orbital-periods Figure 22 shows the relative position errors.

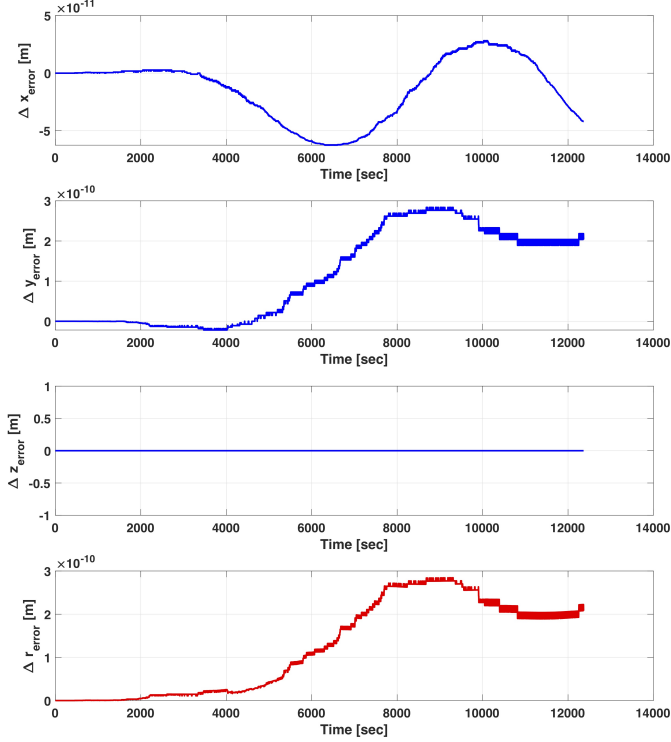


Figure 22. Relative position errors between Hill's Model and Quadratic Drag Model for I.C. = $[-1, 0, 0]$ ($i_{ref} = 70^\circ$ for 2-orbital period) with $\alpha = \beta = 0$ and $h_a = h_p = 902\text{-km}$

4. OPTIMIZATION PROBLEM FORMULATION

This section develops a model of target-chaser rendezvous. The curvilinear LVLH coordinate system described in Section 2 is used for the model formation. We start from the arbitrary relative position and would like to bring the two spacecraft together for docking.

Using the notations described in the beginning of this paper based on full linear model which incorporates both time-averaged J_2 with corrections and quadratic drag perturbations, the dynamics of the two system can now be described as follow. The transnational kinematics and dynamics of a chaser spacecraft in the orbit frame centered at the target vehicle are given by Equation (20),

$$\begin{aligned}\ddot{x} &= 2\omega\dot{y} + (5c^2 - 2)n^2x \\ &\quad - \frac{3n^2J_2R_e^2}{r_{ref}} \left[\frac{1}{2} - \frac{3\sin^2 r_{ref} \sin^2(kt)}{2} - \frac{1 + \cos 2i_{ref}}{8} \right] \\ &\quad - (\beta - \alpha) \left[-\omega^2y + \omega\dot{x} + \left(\frac{\dot{r}_{ref}}{r_{ref}} \right) \omega x + h^{-\frac{1}{2}}r_{ref}\dot{r}_{ref}e^{\alpha\theta}\omega \right] \\ &\quad + f_x\end{aligned}$$

$$\begin{aligned}\ddot{y} &= -2\omega\dot{x} - \frac{3n^2J_2R_e^2}{2r_{ref}} [\sin^2 i_{ref} \sin(2kt)] \\ &\quad + (\beta - \alpha) \left[-\omega^2x - \omega\dot{y} - \left(\frac{\dot{r}_{ref}}{r_{ref}} \right) \omega y - h^{-\frac{1}{2}}r_{ref}^2e^{\alpha\theta}\omega^2 \right] \\ &\quad + f_y \\ \ddot{z} &= -(3c^2 - 2)n^2z - (\beta - \alpha) \left[\omega\dot{z} + \left(\frac{\dot{r}_{ref}}{r_{ref}} \right) \omega z \right] + f_z\end{aligned}\tag{26}$$

where f_x , f_y and f_z are applied forces (controls) expressed in the LVLH frame.

Equation (27) hence defines a 6-state system of differential equations of relative motion governing the rendezvous problem dynamics. Combined into the state vector \mathbf{X} these states are,

$$\mathbf{X} = [x, y, z, \dot{x}, \dot{y}, \dot{z}] \tag{27}$$

The governing dynamics assumes three normalized controls:

$$\mathbf{u} = \left[\frac{f_x}{f_{xmax}} \quad \frac{f_y}{f_{ymax}} \quad \frac{f_z}{f_{zmax}} \right] \tag{28}$$

For simplicity, it is assumed that $f_{imax} = 1\text{m/s}^2$ for $i = x, y, z$. Once again, these controls are three normalized components of a translational force acting on a chaser f_i ($i = x, y, z$), expressed in LVLH coordinate frame. All three controls are bounded: $\mathbf{u}_{min} \leq \mathbf{u} \leq \mathbf{u}_{max}$. The details of the thrust bounds are discussed later with chaser mass and its thrust parameters.

Using the controls the two spacecraft are brought together from some initial condition, given by 6 initial value of states $x_i(t_0)$, $i = 1, \dots, 6$ to docking conditions described by a final state, which for this problem is assumed to be a null i.e. $\mathbf{X}_f = \mathbf{O}$.

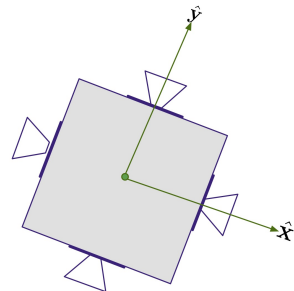


Figure 23. Space vehicle thruster configuration as l^1 norm ²

As the spacecrafts' control and guidance strategies are primarily dictated by the amount of propellant, the proposed control scheme requires the specified mission to be accomplished with the condition of the objective function of propellant minimization. The way this is achieved is by minimizing the total thrust acceleration under the \mathcal{L}^∞ norm of the control. Thrusting here is achieved by six (ungimbled) identical engines rigidly mounted to the body axes as seen in Figure 23. The above is used as the thruster configuration for

²figure courtesy of M. Ross "Space trajectory optimization and \mathcal{L}^∞ optimal control problems"

the secondary spacecraft. Equation (29) now describes the cost functional for the minimization of thrust acceleration.

$$J(\mathbf{f}, \mathbf{u}) = \int_{t_0}^{t_f} (|u_1(t)| + |u_2(t)| + |u_3(t)|) dt \quad (29)$$

Optimization Problem Setup

A sample maneuvering scenario is considered with the chaser center of mass starting at a distance of 1-km behind, 1-km below, and 1-km sideways from the target center of mass. Hence the initial values of the state for computer simulations discussed in the following sections is:

$$\mathbf{X}(t_0) = [-1000, -1000, -1000, 0, 0, 0]^T \quad (30)$$

The endpoint constraint is state constraint at the final time. For simplicity it is assumed that the final state is at the CoM of the target and with null relative velocity vector.

$$\mathbf{X}(t_f) = [0, 0, 0, 0, 0, 0]^T \quad (31)$$

Baseline parameters are selected from a proposed controlled active debris removal (ADR) mission Curimba by Udrea and Nayak [19]. The authors describes Agena-D RBs as one of the potential target for the mission. Hence, the orbital parameters for this upper stage debris corresponds to the reference orbit chosen for this problem. As most of the Agena-D RBs are populated at approximately 70° the reference inclination for this problem is assumed 70° . Additionally, the apogee and the perigee altitude selected for the reference orbit where our target spacecraft is placed resembles that of the Agena-D RB which corresponds to $r_a = 919\text{-km}$ and $r_p = 902\text{-km}$ respectively. Furthermore, a time constraint is added to the simulation by fixing the final time to one-orbital period of the reference orbit, as for the ADR mission it requires the chaser to rendezvous with the target with the shortest amount of time.

The mission proposes a preliminary design of the chaser by considering a 12U CubeSat. This CubeSat is a three-axis stabilized spacecraft of $240 \times 240 \times 360$ mm and a mass of 24 kg. It is known that the CubeSat has a miniaturized system consisting of 16 solenoid-fed thrusters placed such that they generate positive and negative torques about all three body axes with dual redundancy. The thruster arrangement also generates positive and negative forces about two of the three body axes. For the purpose of this work it has been assumed that the force along the third body axis is available when required. Future research will include constraints on the generation of force about the third body axis to take into account the finite slew time.

It is known from the preliminary design provided by the authors that the propellant used will be 1,1-difluoroethane which can generate about 70 s of specific impulse. As for the first mission design iteration they assumed that each thruster produces 50 mN of thrust force [19]. Knowing now the thrust force for individual thrusters (50 mN) and the chaser mass (24 kg), control bounds can be calculated for the optimal problem for the Equation (29). By these means the control bounds thus will be calculated by $\pm \mathbf{F}_T / m_{\text{chaser}}$, where \mathbf{F}_T is the total thrust produced by the chaser spacecraft thrusters. Solving for the control bounds for the defined rendezvous scenario and the assumed chaser parameters gives us: $-8.33 \text{ mm/s}^2 \leq u \leq 8.33 \text{ mm/s}^2$

The above described optimal control problem is solved numerically, by the Gauss Pseudospectral Optimization Solver

(GPOPS) [15]. GPOPS is an open source code that implements a direct collocation method based on the Gauss Pseudospectral approach for solving optimal control problems. It also employed hp-adaptive methods to better approximate the solution by increasing both the order of the fitted polynomial and by increasing the collocation points when needed.

5. SIMULATION RESULTS

The minimum-propellant-control solution with the optimal controls defined in Equation (26) is here presented first. Additionally, the effect of the optimal trajectories with respect to the inclination is discussed, it also shows the effect of the full linear model at different inclinations and how the optimal trajectories are influenced by it. Moreover, linear model without J_2 corrections is formulated and studied to see how the change in the reference orbital period and nodal drift errors affect the optimal solution. Finally, optimization results obtained with Hills equations only are presented and compared.

Minimum Solution for Defined Rendezvous Scenario

For the minimum-propellant-control rendezvous scenario set in Section 4 the pseudospectral method yields the solution shown in Figure 24. Additional planar views of the optimal trajectory is shown in Figure 25.

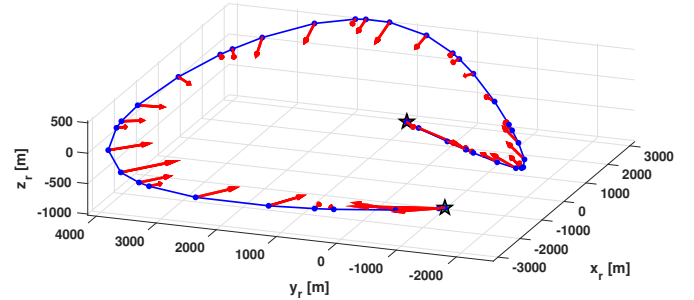


Figure 24. Optimal trajectory for time-averaged J_2 with corrections model ($i_{\text{ref}} = 70^\circ$).

The green marker shows the initial position of the chaser with respect to the target. The final maneuver time as discussed in the previous section is fixed at one orbital period of the reference orbit which when calculated comes to $t_f = 1.72$ hr and ends at the red marker. It is to be noted that the blue markers on the trajectory are the points where the thrust is applied and it is assumed that the thrust applied is impulsively.

Figure 27 shows the time history of the relative position and velocity of the optimal trajectory. Along with that, the control profile for the three normalized components of the thrust force is displayed in Figure 26. It is clearly seen that as there is no significant cross-track motion, the f_z control is not very active. On the other hand, because of the large amplitude of the motion in the radial direction ($\hat{\mathbf{y}}$) and the two rapid consequential change in the radial directions makes the f_y control very active as it maxes out on the thrust bounds.

It should be noted that the relative tolerance of 10^{-3} was set to solve the differential equations. Addition to that the terminal tolerance of the order of 10^{-7} is set for the NLP solved by GPOPS, which does not necessarily indicate the quality of the solution. The reason is that for the solution the parameters of the trajectory are only being computed at 57

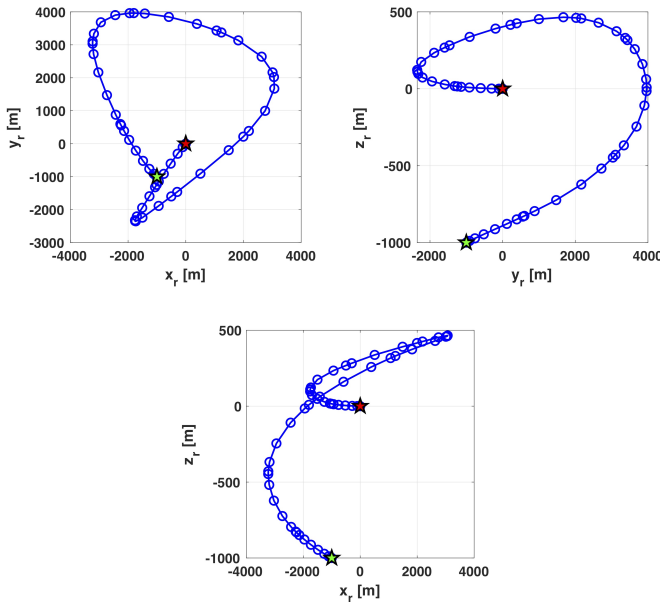


Figure 25. Planar view of the optimal trajectory for Full Linear Model ($i_{ref} = 70^\circ$)

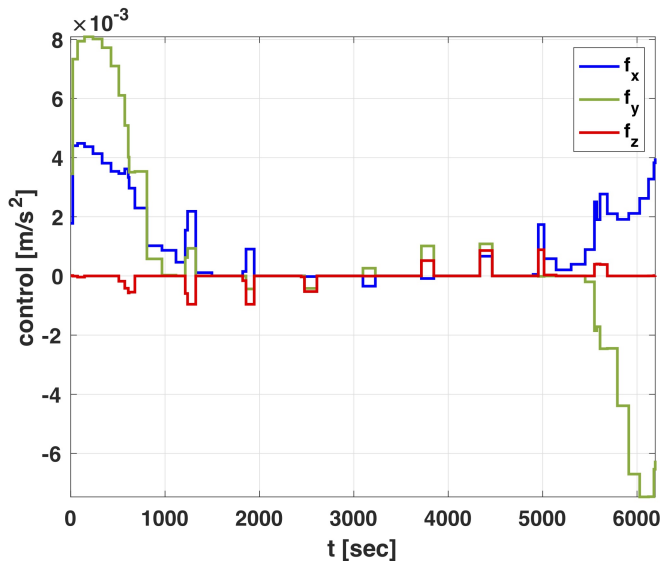


Figure 26. Position and Velocity profiles for the Full Linear Model ($i_{ref} = 70^\circ$)

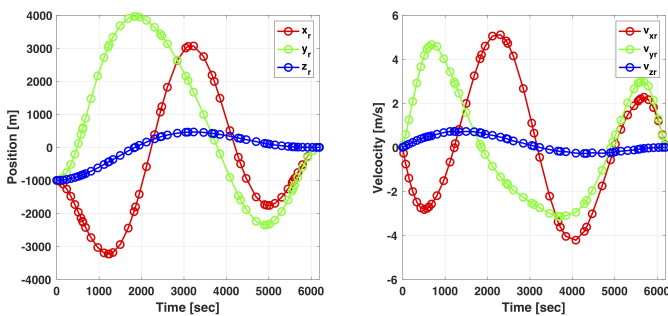


Figure 27. Minimum propellant control profiles for the Full Linear Model ($i_{ref} = 70^\circ$)

nodes only where the optimality conditions are enforced.

For the implementation of the Gauss Pseudospectral method using GPOPS-II the guess for the initial states corresponds to the initial conditions and the guess for the final state consisted of zeros for the entire state. The guess for the control history was zero at the initial and final times for all controls. The solution obtained appears to be feasible but can be used only for offline computations, i.e. on an open-loop guidance scheme.

Minimum Propellant Solution for Hill's Equation

This subsection draws differences in the optimality between the Hill's Equations and the Full Linear Model that integrates both J_2 with corrections and quadratic drag perturbations. The following Figure 28 shows the optimal trajectory for the Hill's equations. As expected a solution similar to Hohmann transfer is achieved. It can be hereby seen that the use of the Hill's equations for the study of optimal trajectories for rendezvous and proximity operations presents very conservative results.

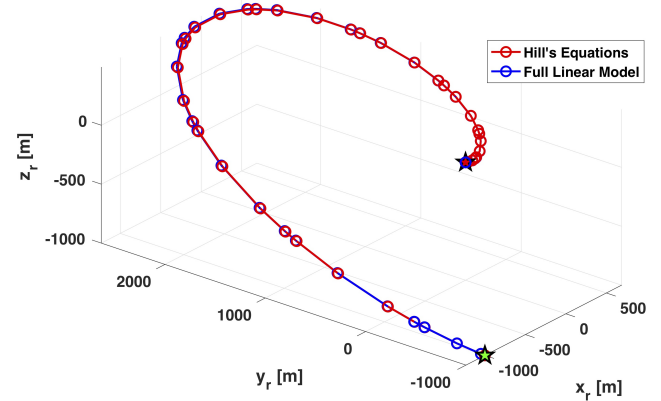


Figure 28. Optimal trajectory for the Hills Equation and the Full Linear Model ($i_{ref} = 0^\circ$ and $\alpha = \beta = 0$).

The above Figure 28 also shows the propellant-optimal trajectories of the full linear model for 0° inclination and assuming the drag constant of both the spacecrafts as zero i.e. $\alpha = \beta = 0$ along with the linearized Hill's equations of motion. Comparing the plotted optimal trajectories validates the correctness of the formulated linear model relative equations. An insignificant error noticed in the relative position is in the same order of magnitude as seen in Figure 21 corresponding to the non circular reference orbit used for the derivation of the full linear model.

Figure 29 and 30 shows a plot of the resulting control history of the three applied thrust forces corresponding to the optimal trajectory shown in Figure 28 using the linearized Hill's equations of motion and the full linear model with perturbations at 0° inclination and zero drag constants. Comparing the identical thrust profiles furthermore validates the correctness of the derived full linear model with perturbations for this study.

Effect of Non Corrected J_2 Perturbation

Figure 31 adds to the study in this section by showing the effect of the differential J_2 without corrections for 70° inclination on the optimal trajectory profile.

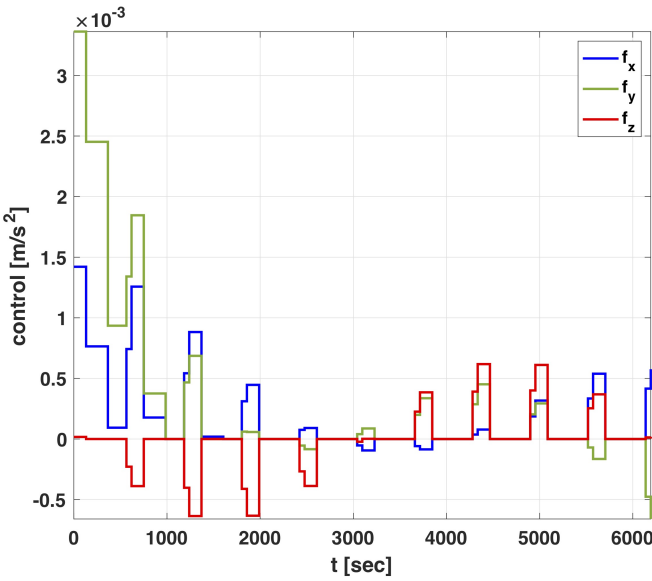


Figure 29. Minimum propellant control profiles for the Full Linear Model for $i_{ref} = 0^\circ$ and $\alpha = \beta = 0$

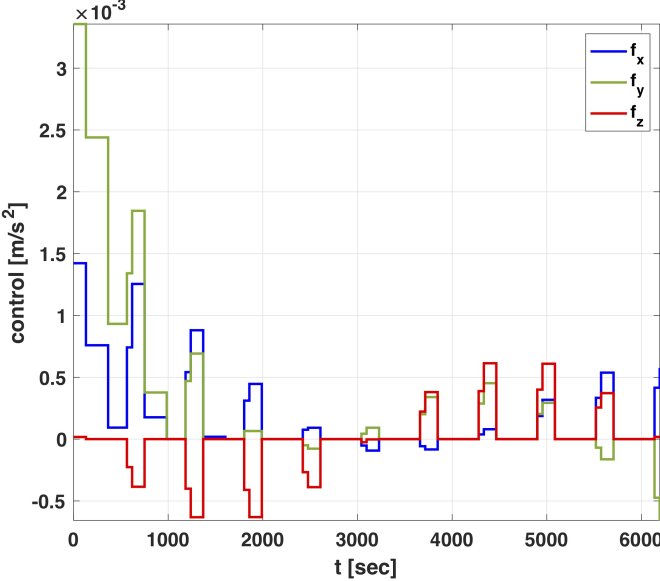


Figure 30. Minimum propellant control profiles for the Hill's Equation

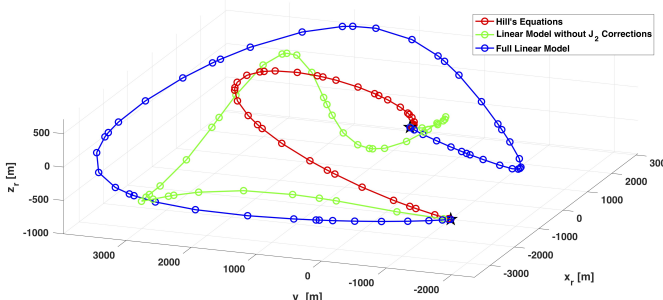


Figure 31. Optimal guidance trajectory for different models ($i_{ref} = 70^\circ$)

This simulated orbit as a part of the optimal solution is along-

side plotted with optimal trajectories of the Full Linear Model that implements all J_2 corrections and the Hill's equations so as to fully understand the sizable errors in the optimal positions caused by the the orbital period mismatch between the target and the chaser orbits and the nodal drift caused by the separation of the ascending node.

Effect of Inclination on the Perturbed Optimal Trajectories

As the effect of J_2 potential is directly proportional to the inclination of the target of the reference orbit. A generalized plot below in shown in Figure 32 that shows the J_2 perturbation effect on the optimal trajectories as the inclination of the reference orbit is increased.

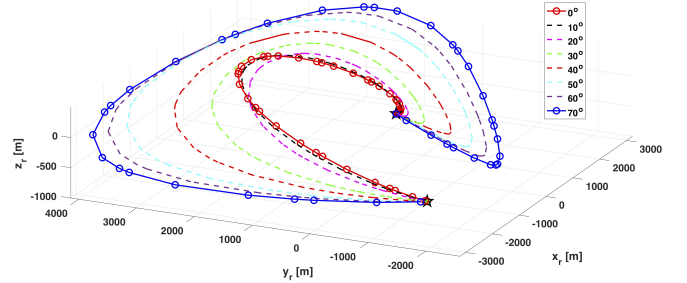


Figure 32. Optimal trajectory for the full linear model for different inclination

It is seen that at lower inclinations the optimal route of the chaser is very similar to that of the Hill's equation which should be the case as we already discussed that the effect of J_2 is not very significant at inclinations near to the equator (0°). For all the simulation plotted in Figure 32, the same rendezvous scenario is considered with fixed final maneuver time of one orbital period.

Effect of Altitude on the Perturbed Optimal Trajectories

Figure 33 shows the effect of altitude on the optimal trajectories. For smaller periods the trajectory profile is very similar. Although, the significance of drag disturbance is truly highlighted by longer period optimal trajectory profiles. Figure 34 shows the optimal profile for 3-orbital period of the reference orbit.

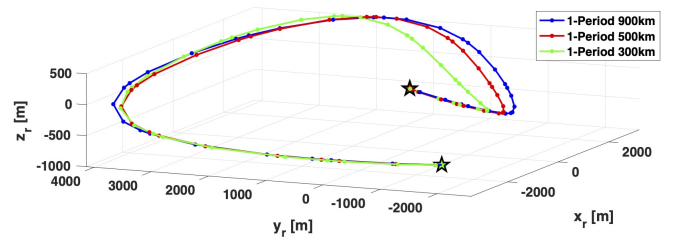


Figure 33. Optimal trajectory for the full linear model for different altitude (1 orbital-period)

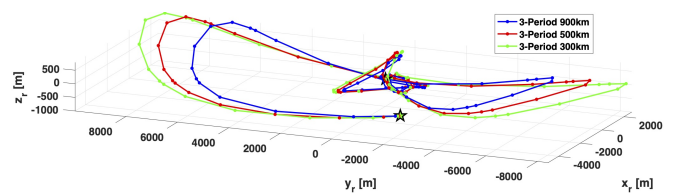


Figure 34. Optimal trajectory for the full linear model for different altitude (3 orbital-period)

An interesting study would be to look at the mapping functions between the optimal profiles obtained above using the full linear model. It can be seen visually that these profiles share a common topological space constrained by initial and final boundary values. In the study of topology, the continuous deformation or a mapping between two function is defined as homotopy. Mapping functions between optimal profiles can help with offline trajectory propagation and for close-loop corrections by attitude control.

6. CONCLUSION

In this paper, the optimal close range rendezvous problem for an ADR spacecraft to approach a tumbling upper stage is formulated and analyzed. A set of new linearized differential equations have been incorporated for describing the relative motion of satellites in the presence of J_2 potential and quadratic drag. Effects on the relative position of the satellite due to time-averaged J_2 with corrections model was shown to advocate its implementation for the proposed optimal propellant rendezvous problem. The minimum-propellant-control problem was formulated and addressed using the direct collocation pseudospectral methods. Differential J_2 without corrections model was all analyzed to show the significant errors in the relative position due to the orbital period mismatch and nodal drifts. The desired optimal trajectory of the chaser spacecraft with respect to the tumbling resident space object is sought such that the desired final state matches its position and velocity under its defined tolerances. The effect of J_2 potential and drag disturbance is examined on the optimality condition for a defined rendezvous scenario.

Further study is required which will incorporate the the full 6dof model of the chaser spacecraft, where both the rotational and transnational dynamics will be considered. Moreover, to make the capture scenario more realistic collision-avoidance condition will be imposed in form of a path constraint. Along with that, docking/capture-enabling conditions will also be incorporated by matching the chaser's and target's docking-station position and velocity vectors. Moreover, optimal-time and optimal-energy conditions will also be studies for the rendezvous scenario to truly find the optimal trajectory for target capture. To study the sensitivity of the initial conditions, control problem will be formulated analytically using an indirect method to better understand the numerical results.

ACKNOWLEDGMENTS

The work presented above benefited greatly by the help of Dr. Anil Rao, Associate Professor at University of Florida, Gainesville for all his time and input with any concerns and questions related to GPOPS-II.

REFERENCES

- [1] Davis, T. M., and Melanson, D., "XSS-10 Micro-Satellite Flght Demonstration Program" Proceedings ogf the 17th Annual AIAA/USU Conference of Small Satellites, Logan, UT, 11-14 Aug. 2003, pp. 99-99.
- [2] David, L., "Military Micro-Sat Explores Space Inspection, Servicing Technologies" Space.com, www.space.com/businesstechnology/050722_xss-11_test.html, Technology, 22 July 2005
- [3] Dornheim, M. A., "Orbital Express to Test Full Autonomy for On-Orbit Service," Aviation Week & Space Technology, www.aviationnow.com/avnow/news/channel_awst_story.jsp?id=news_aw0605_06p1.xml, 4 June 2006 [retrieved 20 July 2009].
- [4] Friend, R. B., "Orbital Express Program Summary and Mission Overview," Proceedings of SPIE: The International Society for Optical Engineering, Vol. 6958, 2008, Paper 695803. doi:10.1117/12.783792
- [5] G. Boyarko, "Spacecraft guidance strategies for proximity maneuvering and close approach with a tumbling object," PhD, 2010.
- [6] G. Boyarko, Y. Oleg, and R. Marcello, "Real-time 6dof guidance for of spacecraft proximity maneuver- ing and close approach with a tumbling object," in 2010 AIAA/AAS Astrodynamics Specialist Conference, ser. Guidance, Navigation, and Control and Co-located Conferences. American Institute of Aeronautics and Astro- nautics, 2010.
- [7] G. Boyarko, O. Yakimenko, and M. Romano, "Optimal rendezvous trajectories of a controlled spacecraft and a tumbling object," Journal of Guidance, Control, and Dynamics, vol. 34, no. 4, pp. 1239–1252, 2011.
- [8] Humi M. and Carter T., "Fuel-Optimal Rendezvous in a Central Force Field with Linear Drag", AAS/AIAA Space Flight Mechanics Meeting, Santa Barbara, California, 2001
- [9] Humi M. and Carter T., "Rendezvous Equations in a Central-Force Field with Linear Drag", Journal of Guid- ance, Contol and Dynamics, Vol. 25, No. 1, Jan.-Feb. 2002
- [10] Humi M. and Carter T., "Clohessy – Wiltshire Equations Modifieed to Include Quadratic Drag",Journal of Guid- ance, Contol and Dynamics, Vol. 25, No. 6, Nov.-Dec. 2002
- [11] Humi M., "Low-Eccentricity Elliptic Orbits in a Central Force Field with Drag", Journal of Guidance, Contol and Dynamics, Vol. 33, No. 5, Sept.-Oct. 2010
- [12] NASA, DART Mission, http://www.nasa.gov/missions-science/dart_into_space.html/
- [13] Patel P., Udrea B. and M. Nayak, "Optimal Guid- ance Trajectories for a Nanosat Docking with a Non- Cooperative Resident Space Object," in 2015 IEEE Aerospace Conference, 2015.
- [14] Prussing, J. E., and Conway, B. A., Orbital Mechanics, Oxford Univ. Press, New York, 1993, pp. 139–169.
- [15] Rao, A. V., Benson, D. A., Darby, C. L., Patterson, M.A., Franscolin, C., Sanders, I., and Huntington, G. T. (2008), "GPOPS: A MATLAB Software for Solving Multiple-Phase Optimal Control Problems Using The Gauss Pseudospectral Method" ACM Transaction on Mathematical Software
- [16] Sedwick, R. J., Miller, D. W., and Kong, E. M. C., "Mitigation of Differential Perturbations in Clusters of Formation Flying Satellites," AAS/AIAA Space Flight Mechanics Meeting, American Astronautical Society, AAS Paper 99-124, Feb. 1999.
- [17] S. Schweighart and R. Sedwick, "High-Fidelity Lin- earized J_2 Model for Satellite Formation Flight.", Journal of Guidance, Control and Dynamics, Vol.25, No.6, Nov-Dec 2002, pp1073-1080
- [18] T. Kasai, M. Oda and T. Suzuki, "Results of the ETS- 7 Mission – Rendezvous Docking and Space Robotics

- Experiment”, in 5th Int. Symp. on Artificial Intelligence, Robotics and Auto. in Space, ESTEC/ESA, Nordwijk, The Netherlands, pp.299-306., 1999.
- [19] B. Udrea, and M. Nayak, “A Cooperative Multi-Satellite Mission for Controlled Active Debris Removal from Low Earth Orbit,” in 2015 IEEE Aerospace Conference, 2015.
- [20] Vallado D.A., Fundamentals of Astrodynamics and Applications, 3rd Edition, Microcosm Press, 2007

BIOGRAPHY



Parv Patel received his B.S. in Aerospace Engineering from Embry-Riddle Aeronautical University, Daytona Beach, FL concentrating in both Astronautics and Propulsion. He further received his M.S. in Astronautical Engineering from the University of Southern California, Los Angeles, CA. He is currently pursuing a Ph.D. degree in Astronautical Engineering at University of Southern California. Parv has worked as a Simulation Test Engineer at Gulfstream Aerospace Corp. Savannah, GA. His research interest include near-Earth object exploration, modeling gravitational fields, interplanetary space mission design, invariant manifolds and spacecraft controls.



Dr. Bogdan Udrea received his Dipl. Eng. in Aeronautical Engineering from the Polytechnic Institute of Bucharest, Romania in 1990 and his Ph.D. in Aeronautics and Astronautics from the University of Washington in 1999. He is the founder and CEO of VisSidus Technologies, Inc., a company that develops technologies for outer space sustainability. Bogdan has a day job as an Associate Professor of Aerospace Engineering at the Embry-Riddle Aeronautical University and has previously worked as a Control and Navigation Systems Engineer at the European Space Agency. His research interests include spacecraft dynamics and control and space mission design with emphasis on proximity operations, formation flying, near-Earth object exploration and on-board autonomy.